

Scan Clusters, Not Pixels: A Cluster-Centric Paradigm for Efficient Ultra-high-definition Image Restoration

Chen Wu¹ Ling Wang² Zhuoran Zheng³ Yuning Cui⁴

Zhixiong Yang¹ Xiangyu Chen⁵ Yue Zhang⁶ Weidong Jiang¹ Jingyuan Xia^{1,*}

¹National University of Defense Technology ²HKUST(GZ) ³Qilu University of Technology

⁴Technical University of Munich ⁵Institute of Artificial Intelligence (TeleAI) ⁶Beihang University

Abstract

Ultra-High-Definition (UHD) image restoration is trapped in a scalability crisis: existing models, bound to pixel-wise operations, demand unsustainable computation. While state space models (SSMs) like Mamba promise linear complexity, their pixel-serial scanning remains a fundamental bottleneck for the millions of pixels in UHD content. We ask: must we process every pixel to understand the image? This paper introduces C²SSM, a visual state space model that breaks this taboo by shifting from pixel-serial to cluster-serial scanning. Our core discovery is that the rich feature distribution of a UHD image can be distilled into a sparse set of semantic centroids via a neural-parameterized mixture model. C²SSM leverages this to reformulate global modeling into a novel dual-path process: it scans and reasons over a handful of cluster centers, then diffuses the global context back to all pixels through a principled similarity distribution, all while a lightweight modulator preserves fine details. This cluster-centric paradigm achieves a decisive leap in efficiency, slashing computational costs while establishing new state-of-the-art results across five UHD restoration tasks. More than a solution, C²SSM charts a new course for efficient large-scale vision: scan clusters, not pixels.

1. Introduction

With the proliferation of mobile devices and streaming media, Ultra-high-definition (UHD, specifically 3840×2160 resolution) imaging has become the dominant paradigm for visual media consumption. However, the pursuit of high-fidelity UHD image restoration (IR) confronts a fundamental and previously unresolved tension: the conflict between the structural redundancy inherent in natural images and the pixel-wise computational primitives employed by contemporary deep models. While State Space Models (SSMs)

like Mamba [7] offer linear complexity for long-range dependency modeling, their core operational unit remains the individual pixel. Applying such pixel-serial scanning mechanisms to UHD images (comprising over 8 million pixels) results in prohibitive memory costs and computational load, exceeding the capacity of consumer-grade GPUs and rendering full-resolution modeling impractical.

Existing attempts to circumvent this bottleneck are fundamentally limited. Multi-scale downsampling methods [15, 27, 34, 42, 43] sacrifice global context and high-frequency details. While SSM-based IR frameworks [8, 9, 46] avoid the quadratic complexity of transformers, they remain bound to pixel- or patch-level scanning, which is intrinsically misaligned with the statistical properties of visual data. These approaches treat pixels as independent entities, failing to capitalize on the underlying low-rank structure and semantic cohesion of image features, thereby incurring substantial and unnecessary computational overhead.

We posit that the key to efficient UHD restoration lies not in faster pixel processing, but in a paradigm shift from pixel-centric to cluster-centric representation. Natural images are not random collections of pixels; they exhibit strong statistical regularities where features converge into a sparse set of semantically coherent regions. Inspired by this, we introduce C²SSM, a novel visual state space model that reformulates image restoration as a process of neural-parameterized mixture distribution modeling and inference.

The core of C²SSM is a theoretically grounded dual-path framework: i) The Cluster-Centric Scanning Module (CCSM) explicitly models the feature distribution via a set of learnable cluster centroids. It constructs an n -dimensional similarity distribution to probabilistically associate each pixel with these centroids, effectively reducing the representation space. Global dependencies are then modeled efficiently by applying the SSM only to the sparse centroids, and the learned contextual weights are propagated back to all pixels through a similarity-guided score diffusion process based on the law of total probability. ii) The Spatial-Channel Feature Modulator (SCFM) acts as an

*Corresponding author.

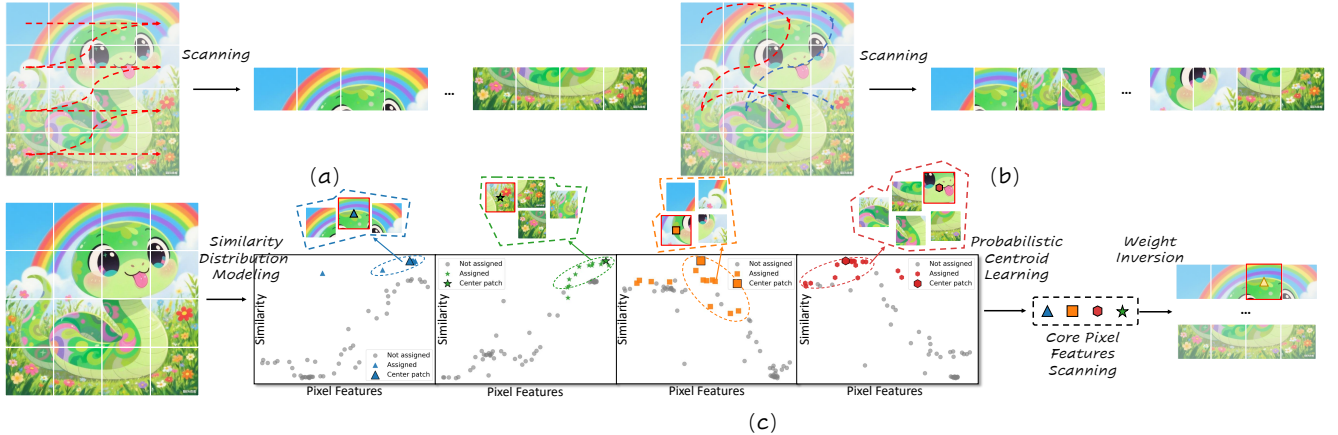


Figure 1. The scanning strategies in existing Mamba-based methods and our proposed method. (a) Vmamba [17] employs a Z-shaped scan path that incurs VRAM bottlenecks when processing UHD images due to its full-pixel scanning. (b) EfficientVMamba [21] reduces scanning costs by omitting sampling steps, this compromises global modeling accuracy. (c) The proposed cluster-centric scanning strategy.

information-theoretic compensator. It operates in parallel to preserve high-frequency details that might be attenuated during clustering. The proposed architectural framework transcends conventional engineering optimizations by introducing a novel probabilistic inference model tailored for visual state space systems. This framework facilitates global reasoning by employing a statistically determined sparse graph composed of centroids, while ensuring the preservation of local fidelity through the modulation of complementary features.

The main contributions of this work are threefold:

- We introduce C^2SSM , the first visual state space model that replaces pixel-level scanning with a cluster-centric probabilistic paradigm. This provides a principled solution to the computational challenges of UHD image restoration.
- We design a novel, theoretically principled dual-path framework. The CCSM provides a low-rank approximation for global context modeling via neural-statistical clustering and differentiable weight inversion, while the SCFM ensures local detail preservation.
- Through extensive experiments on five UHD restoration tasks, we demonstrate that C^2SSM not only achieves state-of-the-art performance but also does so with significantly reduced computational complexity, enabling practical full-resolution restoration on consumer-grade hardware. More importantly, the proposed cluster-centric scanning mechanism offers a new and generalizable direction for efficient large-scale visual computing.

2. Related Work

2.1. State Space Model in Image Restoration

Global receptive fields have proven essential for image restoration tasks [34, 36, 44]. However, Transformer-based

architectures exhibit quadratic computational complexity with respect to input size, resulting in prohibitive computational overhead. Recently, some studies have begun to explore the use of state space models, particularly Mamba, to balance the relationship between efficient computation and direct global receptive fields in restoration tasks. MambaIR [8] applied Visual State Space Models (VSSMs) to image super-resolution, demonstrating competitive performance. MambaIRv2 [9] subsequently resolved inherent causal modeling limitations. Both FreqMamba [47] and FourierMamba [16] employ VSSMs for image deraining in the Fourier domain, with FourierMamba introducing enhanced frequency modeling methods. MaIR [13] introduces locality and continuity properties into VSSMs by refining scanning strategies, delivering promising results across multiple image restoration tasks. Despite achieving linear complexity, these methods still encounter VRAM bottlenecks due to the excessive pixel volume of UHD images, rendering them undeployable on consumer-grade GPUs.

2.2. UHD Image Restoration

UHD image restoration has been an emerging topic in recent years. Early approaches predominantly relied on CNNs. For instance, some works extracted local affine coefficients via CNNs and achieved efficient restoration of degraded UHD images through bilateral learning [42, 43]. DreamUHD [19] and UHD-processor [18] treat the restoration task as a compression-reconstruction task, using re-trained VAE encoders instead of common downsampling. They process features in a downscaled latent space and then reconstruct them. Such methods incur high computational costs, and the two-stage training approach can easily lead to error accumulation. With the success of Transformers in computer vision, researchers began exploring their global modeling capacity for restoration tasks. LLFormer [30]

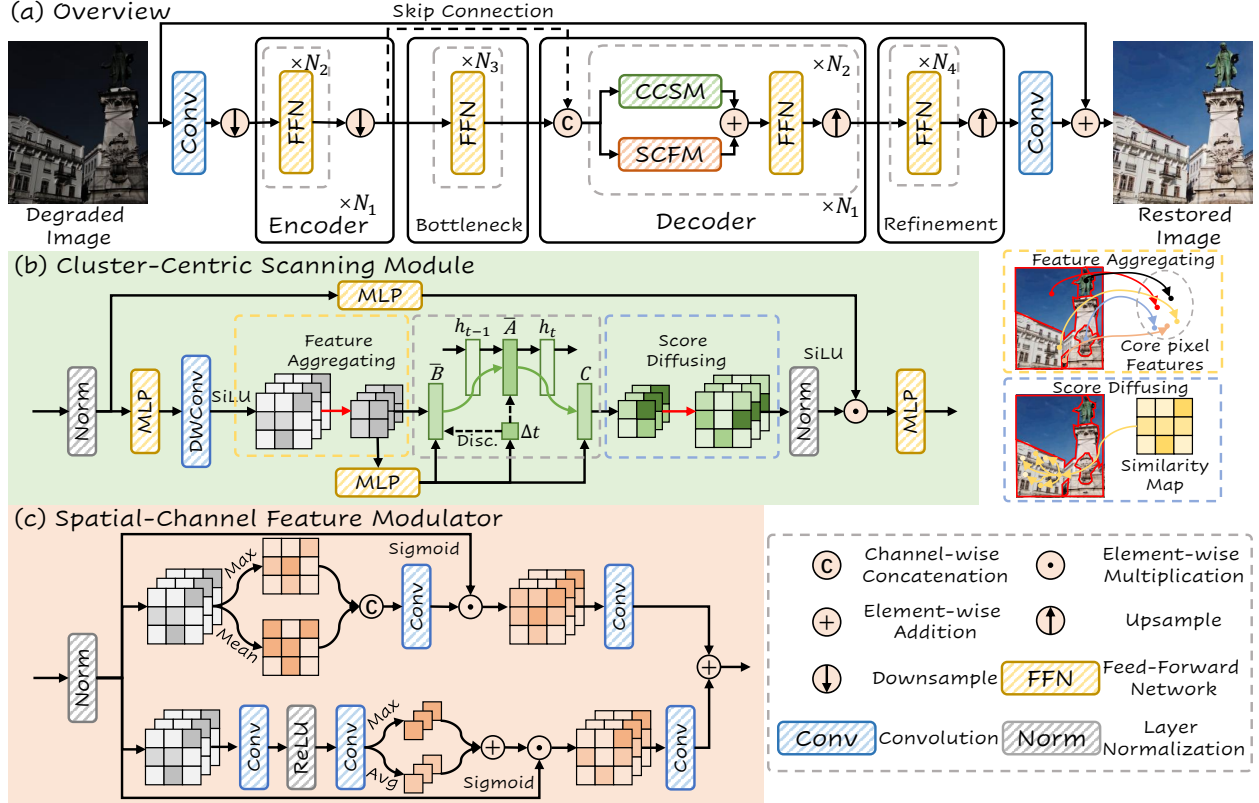


Figure 2. The overview of our proposed C^2SSM . C^2SSM employs an asymmetric U-Net architecture whose decoder integrates the Cluster-Centric Scanning Module and Spatial-Channel Feature Modulator to achieve spatial-channel global feature coupling.

processes UHD images by splitting them into patches for separate restoration before merging, reducing self-attention overhead but introducing boundary artifacts during reconstruction. UHDformer [27] employs a dual-branch strategy, performing global modeling in a highly downsampled low-resolution space. While computationally efficient, this approach discards substantial high-frequency information, compromising restoration quality. The closest work to ours is Wave-Mamba [46], which also leverages a linear-complexity Mamba architecture for long-range modeling. It decomposes images into high/low-frequency components via wavelet transform and models only low-frequency signals. Despite reduced scanning costs, its limited channel capacity (fixed 48 channels throughout the UNet) weakens feature extraction capability, resulting in suboptimal restoration quality. To address this, we propose a novel scanning mechanism for VSSM that revolutionizes full-pixel scanning through cluster-centric point scanning, enabling efficient and effective UHD restoration on consumer-grade GPUs.

3. Methodology

To address the prohibitive quadratic complexity of full-pixel scanning in UHD image restoration, we propose a novel

probability-driven cluster-centric framework for C^2SSM . The core innovation lies in replacing full-pixel traversal with "centroid learning + global weight inversion"—with the critical cluster assignment and centroid refinement both completed in one-step operations—which achieves an acceptable computational overhead while preserving global context.

3.1. Overall Architecture

As illustrated in Fig. 2 (a), the proposed C^2SSM adopts an encoder-decoder architecture where degraded images undergo an N_1 -level restoration pipeline. Each encoder/decoder level contains N_2 basic blocks with convolutional sampling layers (down/up-sampling). Following prior works [11, 45], an asymmetric design is implemented: the encoder comprises only FFNs to reduce computational load, while the decoder, inspired by MetaFormer [38], integrates our CCSM and the SCFM alongside FFNs. A bottleneck layer between the encoder and the decoder allows deep feature extraction, with skip connections via 1×1 convolutions incorporating encoder features into decoder layers. A feature refinement stage post-decoder enhances learned representations, and the final restored image is obtained by adding the learned residual to the degraded input.

3.2. Cluster-Centric Scanning Module

Visual images naturally contain a high degree of semantic redundancy due to the tendency of spatially adjacent areas to share converging feature weight patterns. In addressing this, CCSM employs feature aggregating to concentrate on contextually aggregated significant pixels, thereby substantially decreasing the computational burden associated with global scanning models. Following this, score diffusing enriches the data available for non-essential pixels, facilitating the regional-level reconstruction of entire areas from sparse center points. The CCSM architecture is depicted in Fig. 2 (b). For a layer normalized input feature maps \mathbf{F}_{in} , the calculation of CCSM is updated to:

$$\mathbf{F}_d = \text{SiLU}(\text{DWConv}(\text{MLP}(\mathbf{F}_{in}))), \quad (1)$$

$$\mathbf{F}_f = \text{Norm}(\text{SD}(\text{S6}(\text{FA}(\mathbf{F}_d)))), \quad (2)$$

$$\mathbf{F}_{out} = \mathbf{F}_f \cdot \text{SiLU}(\text{MLP}(\mathbf{F}_{in})), \quad (3)$$

where $\text{SiLU}(\cdot)$ is the SiLU activation functions. $\text{Norm}(\cdot)$ denotes the normalization layer. $\text{FA}(\cdot)$ and $\text{SD}(\cdot)$ are designed feature aggregating and score diffusing, respectively. S6 represents the selective scanning mechanism proposed by Mamba [7].

3.2.1. Feature Aggregating

This stage aims to learn a set of effective, semantically representative centroids from UHD image features, avoiding the inefficiency of random or space-constrained clustering. The key is to model the similarity between pixels and initial centroids as a probabilistic distribution, enabling one-step cross-spatial pixel assignment and one-step adaptive centroid refinement without any iterative processes, ensuring computational efficiency.

Initial Centroid Initialization: Given the layer-normalized feature tensor $F \in \mathbb{R}^{C \times H \times W}$ (output from the encoder), we first select n initial centroids $\{c_1, c_2, \dots, c_n\}$ where $c_k \in \mathbb{R}^{C \times 1 \times 1}$. The initialization follows a uniform sampling strategy across the feature space: we randomly select n pixel positions and calculate their k -nearest neighbor values to enhance local bias. This ensures initial centroids cover diverse feature patterns of the UHD image.

n -Dimensional Similarity Distribution Modeling: For each initial centroid c_k , we compute the cosine similarity between every pixel feature $F_{:,i,j}$ (flattened as f_p to construct a 1-dimensional similarity distribution D_k with c_k). Collectively, the n centroids form an n -dimensional similarity distribution $\mathcal{D} = \{D_1, D_2, \dots, D_n\}$, where each dimension D_k is defined as a probability density function (PDF):

$$p_k(f_p) = \frac{\text{sim}(f_p, c_k)}{\sum_{p \in \Omega} \text{sim}(f_p, c_k)}, \quad (4)$$

where Ω denotes all pixels in the UHD image, and $\text{sim}(\cdot, \cdot)$

is the cosine similarity:

$$\text{sim}(f_p, c_k) = \frac{f_p^T \cdot c_k}{\|f_p\| \cdot \|c_k\|}. \quad (5)$$

For D_k , the horizontal axis represents the feature value of pixels (projected to 1D via PCA for interpretability), and the vertical axis represents the normalized similarity (*i.e.*, the probability that the pixel belongs to the cluster dominated by c_k). This n -dimensional distribution effectively models the semantic correlation between each pixel and the n centroids, transforming pairwise similarity into a probabilistic association.

Centroid Refinement via Learnable Function: For each initial centroid c_k , precomputed similarity distribution $p_k(f_p)$ between the centroid and each pixel feature f_p , the refined centroid \hat{c}_k is obtained through adaptive feature aggregation guided by a learnable gating mechanism. The calculation incorporates two learnable parameters that adjust the sensitivity of similarity-based pixel selection to adapt to diverse feature patterns across different clusters and datasets. Similar to the *qkv* mechanism in self-attention [25], we do not directly compute it; instead, we first use an MLP to map c_k and f_p to v_k and \hat{f}_p , respectively. The refined centroid is formulated as

$$\hat{c}_k = \frac{1}{N_k} \left(v_k + \sum_{p \in \Omega} \delta(\alpha \cdot p_k(f_p) + \beta) \cdot \hat{f}_p \right), \quad (6)$$

where the gating function $\delta(\cdot)$ employs a smooth activation to softly select pixels with meaningful similarity to the initial centroid, balancing selectivity and gradient flow during training. The normalization factor N_k is derived from the sum of activated gating values plus one, ensuring the initial centroid's contribution is retained while scaling the aggregated pixel features to maintain numerical stability. This factor is calculated as

$$N_k = 1 + \sum_{p \in \Omega} \delta(\alpha \cdot p_k(f_p) + \beta). \quad (7)$$

The learnable scaling parameter α modulates the sharpness of similarity-based selection, increasing to enforce stricter relevance thresholds in edge-dominated regions and decreasing to include more diverse features in texture-rich areas. The learnable bias parameter β shifts the activation threshold, adapting to the overall similarity distribution of each cluster to avoid over-pruning or under-selection of relevant pixels. This gating mechanism inherently prunes pixels with insignificant similarity to the centroid, reducing the number of effective computations while preserving semantic relevance.

3.2.2. Score Diffusing

This stage leverages Mamba’s strengths in long-range dependency modeling but only applies it to the n refined centroids (instead of all pixels), then inverts the global pixel weights based on the n -dimensional similarity distribution. The process mimics Transformer’s attention mechanism but avoids full-pixel pairwise computation.

Mamba-Based Centroid Weight Estimation: We feed the refined centroids $\hat{C} = [\hat{c}_1, \hat{c}_2, \dots, \hat{c}_n] \in \mathbb{R}^{C \times n}$ into Mamba’s selective scanning module (S6 block) to learn their precise global weights. Mamba’s state-space modeling efficiently captures long-range dependencies between centroids, outputting a set of centroid-specific weights $W = [w_1, w_2, \dots, w_n] \in \mathbb{R}^{C \times n}$, where w_k denotes the global context weight of centroid \hat{c}_k :

$$W = S6(\hat{C}; \theta_{mamba}). \quad (8)$$

Here, θ_{mamba} are the learnable parameters of the Mamba module. The complexity of this step is $O(C \cdot n^2)$, which is negligible compared to $O(C \cdot H^2W^2)$ for full-pixel scanning (since $n \ll HW$, although there are dimensional transformations in the network that result in an unequal number of channels, all channels are still of the same order of magnitude.)

Weight Inversion via Similarity Distribution: We formalize the assignment probability $\alpha_{p,k}$ of pixel p to cluster k as the posterior probability derived from the n -dimensional similarity distribution \mathcal{D} . Unlike independent parameterization, $\alpha_{p,k}$ is directly normalized from the similarity distribution $p_k(f_p)$ (from Eq. 4) to retain probabilistic consistency:

$$\alpha_{p,k} = \frac{\exp(\alpha \cdot p_k(f_p) + \beta)}{\sum_{k'=1}^n \exp(\alpha \cdot p_{k'}(f_p) + \beta)}. \quad (9)$$

Here, $\alpha_{p,k}$ quantifies the probability that pixel p belongs to the cluster dominated by centroid \hat{c}_k . We adopt softmax normalization to strictly satisfy the probability axiom $\sum_{k=1}^n \alpha_{p,k} = 1$, where α and β are learnable parameters modulating the sharpness of the distribution. This definition directly links the weight inversion to the earlier similarity distribution modeling, forming a closed probabilistic loop. Based on the law of total probability, the global weight w_p of pixel p is the expected value of the centroids’ weights $W = [w_1, w_2, \dots, w_n]$ (from Eq. (8)), conditioned on the pixel’s similarity distribution \mathcal{D} . The inversion formula is thus:

$$w_p = \mathbb{E}_{k \sim \mathcal{D}(p)}[w_k] = \sum_{k=1}^n \alpha_{p,k} \cdot w_k \quad (10)$$

where w_p denotes the global weight of pixel p , and the expectation $\mathbb{E}_{k \sim \mathcal{D}(p)}[w_k]$ explicitly emphasizes that the weight is computed based on the probability distribution of the pixel across the n clusters.

3.3. Spatial-Channel Feature Modulator

To address potential high-frequency detail loss caused by centroid-based aggregation, SCFM operates in parallel with the weight inversion stage. It employs dual-branch attention (spatial + channel) to maximize mutual information between input and output features [33]:

$$W_s = \delta(\text{Conv}([\text{Max}(\mathbf{F}_{in}); \text{Mean}(\mathbf{F}_{in})])), \quad (11)$$

$$F_d = \text{Conv}(\text{ReLU}(\text{Conv}(\mathbf{F}_{in}))), \quad (12)$$

$$W_c = \delta(\text{Max}(F_d) + \text{Avg}(F_d)), \quad (13)$$

$$F_{out} = \text{Conv}(W_s \cdot F_{in}) + \text{Conv}(W_c \cdot F_{in}), \quad (14)$$

where $\text{Max}(\cdot)$ refers to the maximum value operation, while $\text{Mean}(\cdot)/\text{Avg}(\cdot)$ denotes the average value operation. $[\ ; \]$ is the concatenation operation. $\text{ReLU}(\cdot)$ represents ReLU activation function.

4. Experiments

4.1. Experimental Settings

Implementation Details: Our experiments are conducted using PyTorch on a setup of 4 NVIDIA A800 GPUs. To optimize the network, we employ the AdamW optimizer with a initial learning rate 5×10^{-4} and a cosine annealing strategy is used for the decay of the learning rate. We randomly crop the full-resolution 4K image to a resolution of 768×768 as the input and the batch size is set to 16. For all UHD restoration tasks, we perform 150K iterations. To augment the training data, random horizontal and vertical flips are applied to the input images. Our method consists of an encoder-decoder with $N_1 = 3$ levels, where both the encoder and decoder share the same block structure: $N_2 = [2, 4, 4]$. The bottleneck and refinement stages each contain $N_3 = N_5 = 4$ blocks, with a basic embedding dimension of 32. To optimize the weights and biases of the network, we utilize the L1 loss and the FFT loss in the RGB color space as the basic reconstruction loss.

Evaluation: We utilize PSNR [10] and SSIM [31] to assess images with ground truth, while NIQE [20] and PIQE [26] are used for images without it. Elevated PSNR/SSIM values signify enhanced performance, and diminished NIQE/PIQE scores reflect improved quality. Moreover, we compared model parameters across all techniques.

4.2. Comparisons with the State-of-the-art Methods

Low-light Image Enhancement Results: For the task of enhancing UHD images in low-light conditions [15, 30], we evaluate C²SSM against techniques such as Z_DCE++ [14], Uformer [32], Restormer [40], NSEN [39], UHDFour [15], LLFormer [30], UHDformer [27], Wave-Mamba [46], MixNet [34], D2Net [35], UHDDIP [29] and UHD-processor [18]. As evidenced in Tabs. 1 and 2, our method outperforms the current SOTA MixNet by 0.39 dB and

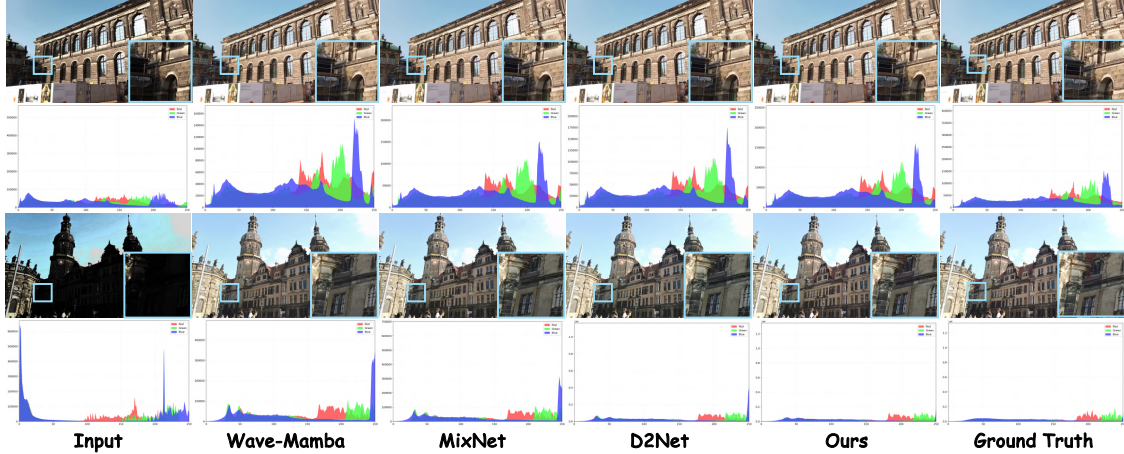


Figure 3. Visual quality comparisons on UHD-LOL4K dataset [30]. The last row shows the color histogram of the image.

Table 1. Comparison of quantitative results on UHD-LOL4K dataset [30].

Methods	Type	Venue	PSNR	SSIM	Param
Z_DCE++ [14]	non-UHD	TPAMI'21	15.58	0.934	79.42K
Uformer [32]		CVPR'22	29.98	0.980	20.63M
Restormer [40]		CVPR'22	36.90	0.988	26.11M
NSEN [39]	UHD	MM'23	29.49	0.980	2.67M
UHDfour [15]		ICLR'23	36.12	0.990	17.54M
LLFormer [30]		AAAI'23	37.33	0.988	24.52M
UHDformer [27]		AAAI'24	36.28	0.989	0.34M
Wave-Mamba [46]		MM'24	37.43	0.990	1.25M
MixNet [34]		NeuroC'24	39.22	0.992	7.77M
D2Net [35]		WACV'25	37.73	0.992	5.22M
ours		-	39.61	0.992	2.71M

Table 2. Comparison of quantitative results on UHD-LL dataset [15].

Methods	Type	Venue	PSNR	SSIM	Param
Z_DCE++ [14]	non-UHD	TPAMI'21	16.41	0.630	10.56K
Uformer [32]		CVPR'22	19.28	0.849	20.63M
Restormer [40]		CVPR'22	22.25	0.871	26.11M
UHDfour [15]	UHD	ICLR'23	26.22	0.900	17.54M
LLFormer [30]		AAAI'23	22.79	0.853	13.15M
UHDformer [27]		AAAI'24	27.11	0.927	0.34M
Wave-Mamba [46]		MM'24	27.35	0.913	1.26M
UHDDIP [29]		TCSVT'25	26.74	0.928	0.81M
MixNet [34]		NeuralC'25	27.54	0.862	7.77M
UHD-processor [18]		CVPR'25	27.22	0.929	1.6M
Ours		-	27.63	0.931	2.71M

0.19 dB in PSNR on synthetic and real-world datasets, respectively. Compared to the Mamba-based method Wave-Mamba, it achieves a significant 2.18 dB improvement. Visual comparisons in Fig. 3 demonstrate that our approach delivers superior color correction, reconstructing images with enhanced visual fidelity and structural clarity.

Image Deraining Results: To validate the effectiveness of our method on the task of rain streak Removal, we compare it with many methods on 4K-Rain13k dataset [1] and 4K-RealRain dataset [1], including RCDNet [28], SPDNet [37], IDT [36], Restormer [40], DRSformer [3], UDR-S2Former [2], NeRD-Rain [4], MambaIRv2 [9],

Table 3. Comparison of quantitative results on 4K-Rain13k dataset [1].

Methods	Type	Venue	PSNR	SSIM	Param
RCDNet [28]	non-UHD	CVPR'20	30.83	0.921	3.17M
SPDNet [37]		ICCV'21	31.81	0.922	3.04M
IDT [36]		TPAMI'22	32.91	0.948	16.41M
Restormer [40]		CVPR'22	33.02	0.934	26.12M
DRSformer [3]		CVPR'23	32.96	0.933	33.65M
UDR-S2Former [2]		ICCV'23	33.36	0.946	8.53M
NeRD-Rain [4]		CVPR'24	33.63	0.935	22.9M
MambaIRv2 [9]		CVPR'25	33.17	0.939	12.7M
UDR-Mixer [1]	UHD	TMM'25	34.30	0.951	4.90M
ERR [41]		CVPR'25	34.48	0.952	1.13M
Ours		-	35.13	0.956	2.71M

UDR-Mixer [1] and ERR [41]. As demonstrated in Tabs. 3 and 4, our method achieves SOTA performance consistently across both synthetic and real-world datasets. Specifically in the 4K-Rain13k dataset, it delivers significant PSNR improvements of 1.96 dB over MambaIRv2 and 0.65 dB over ERR, both Mamba-based methods. Furthermore, visual comparisons in Fig. 4 provide additional validation of our method's efficacy.

Image Deblurring Results: In the UHD image deblurring task [27], we evaluate our proposed C²SSM against existing deblurring approaches, including MIMO-Unet++ [5], Restormer [40], Uformer [32], Stripformer [24], FFTformer [11], UHDformer [27], UHDDIP [29], DreamUHD [19], UHD-processor [18] and ERR [41]. As quantified in Tab. 5, our method achieves a significant 1.81 dB PSNR advantage over the top-performing baseline ERR. Visual evidence in Fig. 5 corroborates that our reconstructions exhibit superior structural integrity and visual naturalness.

Image Dehazing Results: For UHD image dehazing task [27], we compare our C²SSM with a wide range of state-of-the-art methods, including Restormer [40], Uformer [32], DehazeFormer [23], MB-TaylorFormer [22], UHD [43], UHDformer [27], UHDDIP [29] and UHD-processor [18]. As shown in Tab. 6, our method achieves

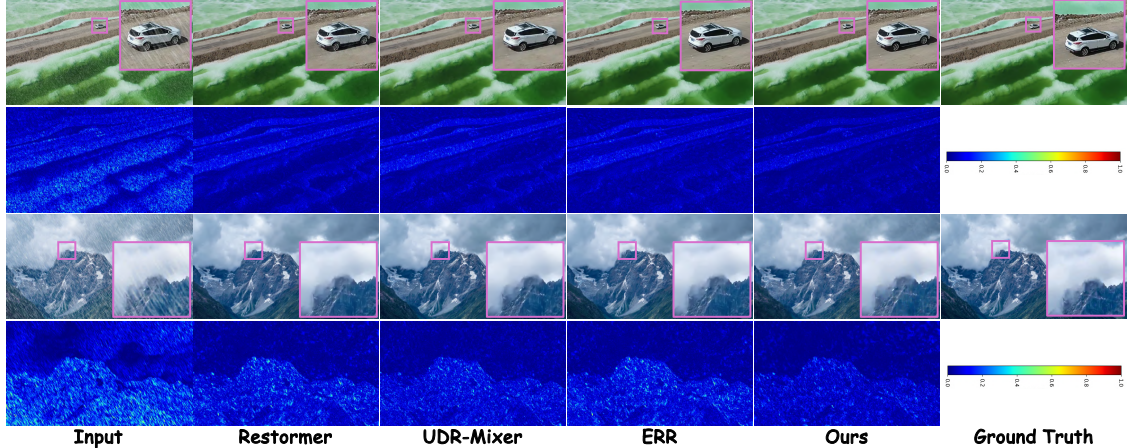


Figure 4. Visual quality comparisons on 4K-Rain13k dataset [1]. The last row shows the error map of the image.

Table 4. Comparison of quantitative results on 4K-RealRain dataset [1].

Methods	RCDNet [28]	SPDNet [37]	IDT [36]	Restormer [40]	DRSformer [3]	NeRD-Rain [4]	MambaIRv2 [9]	ERR [41]	Ours
NIQE	9.997	9.917	9.067	8.636	8.49	9.139	9.397	9.136	8.198
PIQE	63.816	64.774	<u>55.049</u>	60.335	60.441	60.070	62.913	59.735	54.90

Table 5. Comparison of quantitative results on UHD-Blur dataset [27].

Methods	Type	Venue	PSNR	SSIM	Param
MIMO-Unet++ [5]	non-UHD	ICCV'21	25.03	0.752	16.1M
Restormer [40]		CVPR'22	25.21	0.752	26.1M
Uformer [32]		CVPR'22	25.27	0.752	20.6M
Stripformer [24]		ECCV'22	25.05	0.750	19.7M
FFTformer [11]		CVPR'23	25.41	0.757	16.6M
UHDformer [27]	UHD	AAAI'24	28.82	0.844	0.34M
UHDDIP [29]		TCSVT'25	28.28	0.845	0.81M
DreamUHD [19]		AAAI'25	29.33	0.852	1.45M
UHD-processor [18]		CVPR'25	29.43	0.855	1.6M
ERR [41]		CVPR'25	<u>29.72</u>	0.861	1.13M
Ours		-	31.53	0.890	2.71M

favorable results in quantitative metrics compared to existing approaches.

Image Desnowing Results: In the image desnowing task, we compare HiFormer with Uformer [32], Restormer [40], SFNet [6], UHD [43], UHDformer [27], and UHDDIP [29]. As shown in Tab. 7, our method exceeds the current best-performing method, UHDDIP, by 1.5 dB in PSNR.

4.3. Ablation Studies and Discussions

We further conduct extensive ablation studies to better understand and evaluate each component in the proposed C²SSM. For a fair comparison, all these variants are trained using the same settings.

Effectiveness of Proposed Blocks: To assess the contribution of the proposed CCSM and SCFM to overall framework performance, we design a series of ablative variants involving their systematic removal or functional substitution, thereby rigorously quantifying their efficacy. As shown in Tab. 8, removing or replacing the proposed modules leads to performance degradation, confirming their effectiveness. Notably, due to computational complexity

Table 6. Comparison of quantitative results on UHD-Haze dataset [27].

Methods	Type	Venue	PSNR	SSIM	Param
Restormer [40]	non-UHD	CVPR'22	12.72	0.693	26.11M
Uformer [32]		CVPR'22	19.83	0.737	20.63M
DehazeFormer [23]		TIP'23	15.37	0.725	2.5M
MB-TaylorFormer [22]		ICCV'23	20.99	0.919	2.7M
UHD [43]	UHD	ICCV'21	18.04	0.811	34.5M
UHDformer [27]		AAAI'24	22.59	<u>0.942</u>	0.34M
UHDDIP [29]		TCSVT'25	22.14	0.941	0.81M
UHD-processor [18]		CVPR'25	<u>23.24</u>	0.953	1.6M
Ours		-	24.08	<u>0.942</u>	2.71M

Table 7. Comparison of quantitative results on UHD-Snow dataset [29].

Methods	Type	Venue	PSNR	SSIM	Param
Uformer [32]	non-UHD	CVPR'22	23.71	0.871	20.63M
Restormer [40]		CVPR'22	24.14	0.869	26.12M
SFNet [6]		ICLR'23	23.63	0.845	7.05M
UHD [43]	UHD	ICCV'21	29.29	0.949	34.5M
UHDformer [27]		AAAI'24	36.61	0.988	0.34M
UHDDIP [29]		TCSVT'25	<u>41.56</u>	0.990	0.81M
Ours		-	42.45	0.990	2.71M

constraints, both vanilla Mamba and ASSM are incapable of full-resolution inference on consumer-grade hardware, necessitating aggressive downsampling (typically 8×) for UHD image preprocessing, followed by upsampling to restore the original resolution. This compulsory resolution compromise not only introduces additional information loss but also limits the model's capacity to preserve high-frequency details. In contrast, our CCSM, through its sparse representation mechanism based on cluster centroids, successfully achieves full-resolution processing while maintaining feasible computational overhead, fundamentally addressing the memory bottleneck in UHD image restoration. The most significant performance drop occurs when CCSM is removed, demonstrating that long-range depen-

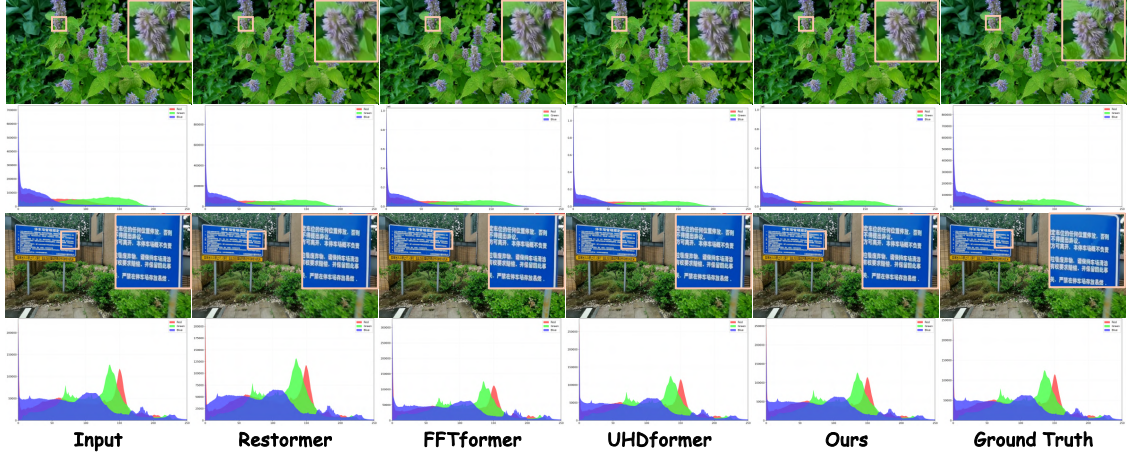


Figure 5. Visual quality comparisons on UHD-Blur dataset [27]. The last row shows the color histogram of the image.

Table 8. Ablation study of proposed blocks on UHD-LOL4K dataset [30].

Variants	PSNR	SSIM	Param
(a) replace CCSM with ResBlock	37.32	0.989	2.38M
(b) replace CCSM with Vanilla Mamba [8]	37.43	0.990	3.11M
(c) replace CCSM with ASSM [9]	38.71	0.991	2.96M
(d) replace SCFM with ResBlock	39.25	0.992	2.69M
(e) remove CCSM	35.87	0.987	2.21M
(f) remove SCFM	39.05	0.992	2.53M
(g) full model (ours)	39.61	0.992	2.71M

dependency modeling is crucial for the restoration task. Furthermore, CCSM proves superior to SCFM in importance, as SCFM essentially serves as a supplementary module to compensate for information loss caused by incomplete global modeling in CCSM.

Validation of the Number of Centers: To investigate the impact of cluster center quantity on model performance, we conduct experiments on UHD-LOL4K, UHD-Blur, and UHD-Haze datasets. Results in Tab. 9 demonstrate that setting the number of centers to 4 achieves optimal balanced performance across multiple datasets. As the center count increases, average performance slightly declines, potentially due to redundant clusters affecting results. Notably, the UHD-Blur dataset attains peak performance with 6 centers, which may be attributed to its inherent dataset bias: consisting predominantly of indoor and complex scenes with high content diversity, demanding more complex representations. In contrast, UHD-LOL4K and UHD-Haze primarily contain outdoor scenes featuring extensive homogeneous regions such as skies and ground planes.

Comparison with Other Scanning Strategy: To validate the efficiency of our proposed scanning strategy, we compare computational complexity with various Mamba-based methods. While MambaIR [8] and Wave-Mamba [46] employ vanilla scanning strategies, both EVSSM [12] and MambaIRv2 [9] implement customized scanning designs. As demonstrated in Tab. 10, our approach achieves the low-

Table 9. Ablation study of the number of centers.

Number of Centers	2	4	6	8
UHD-LOL4K [30]	37.91/0.992	39.61/0.992	39.23/0.992	39.19/0.992
UHD-Blur [27]	30.42/0.881	31.53/0.890	31.72/0.890	31.65/0.889
UHD-Haze [27]	23.27/0.940	24.08/0.942	24.03/0.942	23.86/0.942

Table 10. Comparison of different scanning strategies. FLOPs are measured with an image of the size 64×64 pixels.

Method	MambaIR [8]	Wave-Mamba [46]	EVSSM [12]	MambaIRv2 [9]	Ours
Param	1.32M	1.25M	17.13M	0.84M	2.71M
FLOPs	4.774G	0.881G	7.893G	4.940G	0.407G
Venue	ECCV'24	MM'24	CVPR'25	CVPR'25	-

est computational complexity. It is worth noting that, except for Wave-Mamba, these methods cannot perform full-resolution inference on UHD images, so we do not report their performance uniformly. You can find the comparison results of Wave-Mamba and MambaIRv2 with our method in Tab. 1, 2, 3 and 4. Collectively, the CCSM design enables our method to maintain outstanding performance while significantly reducing computational overhead.

5. Conclusion

In this paper, we proposed C^2SSM , a novel visual state space model that breaks the computational bottlenecks of existing mamba-based methods in UHD image restoration by shifting from pixel-serial to cluster-serial scanning. The core of C^2SSM lies in the CCSM, which models UHD images as a sparse set of semantic centroids. By performing global reasoning only on these centroids and diffusing the learned context back to pixels via a principled similarity distribution, CCSM achieves a dramatic reduction in computational complexity without sacrificing performance. Complementing this, the SCFM ensures the preservation of high-frequency details that may be overlooked during clustering. CCSM and SCFM complement each other. Comprehensive experiments across numerous UHD image restoration tasks reveal our method surpasses current SOTA methods in both quantitative metrics and qualitative analysis.

References

- [1] Hongming Chen, Xiang Chen, Chen Wu, Zhuoran Zheng, Jinshan Pan, and Xianping Fu. Towards ultra-high-definition image deraining: A benchmark and an efficient method. *arXiv preprint arXiv:2405.17074*, 2024. 6, 7
- [2] Sixiang Chen, Tian Ye, Jinbin Bai, Erkang Chen, Jun Shi, and Lei Zhu. Sparse sampling transformer with uncertainty-driven ranking for unified removal of raindrops and rain streaks. In *Proceedings of the IEEE/CVF International Conference on Computer Vision*, pages 13106–13117, 2023. 6
- [3] Xiang Chen, Hao Li, Mingqiang Li, and Jinshan Pan. Learning a sparse transformer network for effective image deraining. In *Proceedings of the IEEE/CVF Conference on Computer Vision and Pattern Recognition*, pages 5896–5905, 2023. 6, 7
- [4] Xiang Chen, Jinshan Pan, and Jiangxin Dong. Bidirectional multi-scale implicit neural representations for image deraining. In *Proceedings of the IEEE/CVF conference on computer vision and pattern recognition*, pages 25627–25636, 2024. 6, 7
- [5] Sung-Jin Cho, Seo-Won Ji, Jun-Pyo Hong, Seung-Won Jung, and Sung-Jea Ko. Rethinking coarse-to-fine approach in single image deblurring. In *Proceedings of the IEEE/CVF international conference on computer vision*, pages 4641–4650, 2021. 6, 7
- [6] Yuning Cui, Yi Tao, Zhenshan Bing, Wenqi Ren, Xinwei Gao, Xiaochun Cao, Kai Huang, and Alois Knoll. Selective frequency network for image restoration. In *The eleventh international conference on learning representations*, 2023. 7
- [7] Albert Gu and Tri Dao. Mamba: Linear-time sequence modeling with selective state spaces. *arXiv preprint arXiv:2312.00752*, 2023. 1, 4
- [8] Hang Guo, Jinmin Li, Tao Dai, Zhihao Ouyang, Xudong Ren, and Shu-Tao Xia. Mambair: A simple baseline for image restoration with state-space model. In *European conference on computer vision*, pages 222–241. Springer, 2024. 1, 2, 8
- [9] Hang Guo, Yong Guo, Yaohua Zha, Yulun Zhang, Wenbo Li, Tao Dai, Shu-Tao Xia, and Yawei Li. Mambairv2: Attentive state space restoration. In *Proceedings of the Computer Vision and Pattern Recognition Conference*, pages 28124–28133, 2025. 1, 2, 6, 7, 8
- [10] Quan Huynh-Thu and Mohammed Ghanbari. Scope of validity of psnr in image/video quality assessment. *Electronics letters*, 44(13):800–801, 2008. 5
- [11] Lingshun Kong, Jiangxin Dong, Jianjun Ge, Mingqiang Li, and Jinshan Pan. Efficient frequency domain-based transformers for high-quality image deblurring. In *Proceedings of the IEEE/CVF Conference on Computer Vision and Pattern Recognition*, pages 5886–5895, 2023. 3, 6, 7
- [12] Lingshun Kong, Jiangxin Dong, Jinhui Tang, Ming-Hsuan Yang, and Jinshan Pan. Efficient visual state space model for image deblurring. In *Proceedings of the Computer Vision and Pattern Recognition Conference*, pages 12710–12719, 2025. 8
- [13] Boyun Li, Haiyu Zhao, Wenxin Wang, Peng Hu, Yuanbiao Gou, and Xi Peng. Mair: A locality-and continuity-preserving mamba for image restoration. In *Proceedings of the Computer Vision and Pattern Recognition Conference*, pages 7491–7501, 2025. 2
- [14] Chongyi Li, Chunle Guo, and Chen Change Loy. Learning to enhance low-light image via zero-reference deep curve estimation. *IEEE Transactions on Pattern Analysis and Machine Intelligence*, 44(8):4225–4238, 2021. 5, 6
- [15] Chongyi Li, Chun-Le Guo, Man Zhou, Zhixin Liang, Shangchen Zhou, Ruicheng Feng, and Chen Change Loy. Embedding fourier for ultra-high-definition low-light image enhancement. *arXiv preprint arXiv:2302.11831*, 2023. 1, 5, 6
- [16] Dong Li, Yidi Liu, Xueyang Fu, Senyan Xu, and Zheng-Jun Zha. Fouriermamba: Fourier learning integration with state space models for image deraining. *arXiv preprint arXiv:2405.19450*, 2024. 2
- [17] Yue Liu, Yunjie Tian, Yuzhong Zhao, Hongtian Yu, Lingxi Xie, Yaowei Wang, Qixiang Ye, Jianbin Jiao, and Yunfan Liu. Vmamba: Visual state space model. *Advances in neural information processing systems*, 37:103031–103063, 2024. 2
- [18] Yidi Liu, Dong Li, Xueyang Fu, Xin Lu, Jie Huang, and Zheng-Jun Zha. Uhd-processor: Unified uhd image restoration with progressive frequency learning and degradation-aware prompts. In *Proceedings of the Computer Vision and Pattern Recognition Conference*, pages 23121–23130, 2025. 2, 5, 6, 7
- [19] Yidi Liu, Dong Li, Jie Xiao, Yuanfei Bao, Senyan Xu, and Xueyang Fu. Dreamuhd: Frequency enhanced variational autoencoder for ultra-high-definition image restoration. In *Proceedings of the AAAI Conference on Artificial Intelligence*, pages 5712–5720, 2025. 2, 6, 7
- [20] Anish Mittal, Anush Krishna Moorthy, and Alan Conrad Bovik. No-reference image quality assessment in the spatial domain. *IEEE Transactions on image processing*, 21(12):4695–4708, 2012. 5
- [21] Xiaohuan Pei, Tao Huang, and Chang Xu. Efficientvmamba: Atrous selective scan for light weight visual mamba. In *Proceedings of the AAAI Conference on Artificial Intelligence*, pages 6443–6451, 2025. 2
- [22] Yuwei Qiu, Kaihao Zhang, Chenxi Wang, Wenhan Luo, Hongdong Li, and Zhi Jin. Mb-taylorformer: Multi-branch efficient transformer expanded by taylor formula for image dehazing. In *Proceedings of the IEEE/CVF international conference on computer vision*, pages 12802–12813, 2023. 6, 7
- [23] Yuda Song, Zhuqing He, Hui Qian, and Xin Du. Vision transformers for single image dehazing. *IEEE Transactions on Image Processing*, 32:1927–1941, 2023. 6, 7
- [24] Fu-Jen Tsai, Yan-Tsung Peng, Yen-Yu Lin, Chung-Chi Tsai, and Chia-Wen Lin. Stripformer: Strip transformer for fast image deblurring. In *European conference on computer vision*, pages 146–162. Springer, 2022. 6, 7
- [25] Ashish Vaswani, Noam Shazeer, Niki Parmar, Jakob Uszkoreit, Llion Jones, Aidan N Gomez, Łukasz Kaiser, and Illia Polosukhin. Attention is all you need. *Advances in neural information processing systems*, 30, 2017. 4

- [26] Narasimhan Venkatanath, D Praneeth, S Channappayya Sumohana, S Medasani Swarup, et al. Blind image quality evaluation using perception based features. In *2015 twenty first national conference on communications (NCC)*, pages 1–6. IEEE, 2015. 5
- [27] Cong Wang, Jinshan Pan, Wei Wang, Gang Fu, Siyuan Liang, Mengzhu Wang, Xiao-Ming Wu, and Jun Liu. Correlation matching transformation transformers for uhd image restoration. In *Proceedings of the AAAI Conference on Artificial Intelligence*, pages 5336–5344, 2024. 1, 3, 5, 6, 7, 8
- [28] Hong Wang, Qi Xie, Qian Zhao, and Deyu Meng. A model-driven deep neural network for single image rain removal. In *Proceedings of the IEEE/CVF conference on computer vision and pattern recognition*, pages 3103–3112, 2020. 6, 7
- [29] Liyan Wang, Cong Wang, Jinshan Pan, Xiaofeng Liu, Weixiang Zhou, Xiaoran Sun, Wei Wang, and Zhixun Su. Ultra-high-definition image restoration: New benchmarks and a dual interaction prior-driven solution. *arXiv preprint arXiv:2406.13607*, 2024. 5, 6, 7
- [30] Tao Wang, Kaihao Zhang, Tianrun Shen, Wenhan Luo, Bjorn Stenger, and Tong Lu. Ultra-high-definition low-light image enhancement: A benchmark and transformer-based method. In *Proceedings of the AAAI Conference on Artificial Intelligence*, pages 2654–2662, 2023. 2, 5, 6, 8
- [31] Zhou Wang, Alan C Bovik, Hamid R Sheikh, and Eero P Simoncelli. Image quality assessment: from error visibility to structural similarity. *IEEE transactions on image processing*, 13(4):600–612, 2004. 5
- [32] Zhendong Wang, Xiaodong Cun, Jianmin Bao, Wengang Zhou, Jianzhuang Liu, and Houqiang Li. Uformer: A general u-shaped transformer for image restoration. In *Proceedings of the IEEE/CVF conference on computer vision and pattern recognition*, pages 17683–17693, 2022. 5, 6, 7
- [33] Sanghyun Woo, Jongchan Park, Joon-Young Lee, and In So Kweon. Cbam: Convolutional block attention module. In *Proceedings of the European conference on computer vision (ECCV)*, pages 3–19, 2018. 5
- [34] Chen Wu, Zhuoran Zheng, Xiuyi Jia, and Wenqi Ren. Mixnet: Towards effective and efficient uhd low-light image enhancement. *arXiv preprint arXiv:2401.10666*, 2024. 1, 2, 5, 6
- [35] Chen Wu, Ling Wang, Long Peng, Dianjie Lu, and Zhuoran Zheng. Dropout the high-rate downsampling: A novel design paradigm for uhd image restoration. In *2025 IEEE/CVF Winter Conference on Applications of Computer Vision (WACV)*, pages 2390–2399. IEEE, 2025. 5, 6
- [36] Jie Xiao, Xueyang Fu, Aiping Liu, Feng Wu, and Zheng-Jun Zha. Image de-raining transformer. *IEEE Transactions on Pattern Analysis and Machine Intelligence*, 45(11):12978–12995, 2022. 2, 6, 7
- [37] Qiaosi Yi, Juncheng Li, Qinyan Dai, Faming Fang, Guixu Zhang, and Tiejong Zeng. Structure-preserving deraining with residue channel prior guidance. In *Proceedings of the IEEE/CVF international conference on computer vision*, pages 4238–4247, 2021. 6, 7
- [38] Weihao Yu, Mi Luo, Pan Zhou, Chenyang Si, Yichen Zhou, Xinchao Wang, Jiashi Feng, and Shuicheng Yan. Metaformer is actually what you need for vision. In *Proceedings of the IEEE/CVF conference on computer vision and pattern recognition*, pages 10819–10829, 2022. 3
- [39] Wei Yu, Qi Zhu, Naishan Zheng, Jie Huang, Man Zhou, and Feng Zhao. Learning non-uniform-sampling for ultra-high-definition image enhancement. In *Proceedings of the 31st ACM International Conference on Multimedia*, pages 1412–1421, 2023. 5, 6
- [40] Syed Waqas Zamir, Aditya Arora, Salman Khan, Munawar Hayat, Fahad Shahbaz Khan, and Ming-Hsuan Yang. Restormer: Efficient transformer for high-resolution image restoration. In *Proceedings of the IEEE/CVF conference on computer vision and pattern recognition*, pages 5728–5739, 2022. 5, 6, 7
- [41] Chen Zhao, Zhizhou Chen, Yunzhe Xu, Enxuan Gu, Jian Li, Zili Yi, Qian Wang, Jian Yang, and Ying Tai. From zero to detail: Deconstructing ultra-high-definition image restoration from progressive spectral perspective. *arXiv preprint arXiv:2503.13165*, 2025. 6, 7
- [42] Zhuoran Zheng, Wenqi Ren, Xiaochun Cao, Xiaobin Hu, Tao Wang, Fenglong Song, and Xiuyi Jia. Ultra-high-definition image dehazing via multi-guided bilateral learning. In *2021 IEEE/CVF Conference on Computer Vision and Pattern Recognition (CVPR)*, pages 16180–16189. IEEE, 2021. 1, 2
- [43] Zhuoran Zheng, Wenqi Ren, Xiaochun Cao, Tao Wang, and Xiuyi Jia. Ultra-high-definition image hdr reconstruction via collaborative bilateral learning. In *Proceedings of the IEEE/CVF international conference on computer vision*, pages 4449–4458, 2021. 1, 2, 6, 7
- [44] Man Zhou, Jie Huang, Chun-Le Guo, and Chongyi Li. Fourmer: An efficient global modeling paradigm for image restoration. In *International conference on machine learning*, pages 42589–42601. PMLR, 2023. 2
- [45] Shihao Zhou, Duosheng Chen, Jinshan Pan, Jinglei Shi, and Jufeng Yang. Adapt or perish: Adaptive sparse transformer with attentive feature refinement for image restoration. In *Proceedings of the IEEE/CVF conference on computer vision and pattern recognition*, pages 2952–2963, 2024. 3
- [46] Wenbin Zou, Hongxia Gao, Weipeng Yang, and Tongtong Liu. Wave-mamba: Wavelet state space model for ultra-high-definition low-light image enhancement. In *Proceedings of the 32nd ACM International Conference on Multimedia*, pages 1534–1543, 2024. 1, 3, 5, 6, 8
- [47] Zhen Zou, Hu Yu, Jie Huang, and Feng Zhao. Freqmamba: Viewing mamba from a frequency perspective for image deraining. In *Proceedings of the 32nd ACM international conference on multimedia*, pages 1905–1914, 2024. 2